RSC Advances

PAPER

View Article Online
View Journal | View Issue

Cite this: *RSC Adv.*, 2015, **5**, 17018

Catalytic performance of $CuO/Ce_{0.8}Zr_{0.2}O_2$ loaded onto SiC-DPF in NO_x-assisted combustion of diesel soot

Susana Quiles-Díaz, Javier Giménez-Mañogil and Avelina García-García*

This work presents a comparative study between the catalytic performance of the 2% CuO/ceria-zirconia powder catalyst and the same catalyst supported on silicon carbide DPF (Diesel Particulate Filter) towards NO oxidation reaction and soot combustion reaction. The ceria-zirconia catalyst was prepared by the co-precipitation method and 2 wt% copper was incorporated by the incipient wetness impregnation method. The catalyst was incorporated onto the ceramic support using a simple and organic solvent-free procedure by a simply dipping the DPF into an aqueous solution of the catalyst. The powder catalyst has been characterized using N_2 adsorption at −196 °C, XRD and Raman Spectroscopy; whereas the catalytic coating morphology has been evaluated by SEM and the mechanical stability by an adherence test. Both catalyst configurations were tested for NO oxidation to NO_2 and for soot combustion under NO_x/O_2. The results revealed that incorporation of the very active copper/ceria-zirconia catalyst onto SiC-DPF has been successfully achieved by a simple coating procedure. Furthermore, the catalytic coating has shown suitable mechanical, chemical and thermal stability. A satisfactory catalytic performance of the catalytic-coated filter was reached towards the NO oxidation reaction. Moreover, it was proved that the catalytic coating is stable and the corresponding coated DPF can be reused for several cycles of NO oxidation without a significant decrease in its activity. Finally, it was verified that the loose-contact mode is a good choice to simulate the catalytic performance of this active phase in a real diesel particulate filter.

Received 1st December 2014
Accepted 2nd February 2015

DOI: 10.1039/c4ra15595e

www.rsc.org/advances

1. Introduction

The majority of environmental pollutants released to the atmosphere come from fossil fuels' inefficient combustion.[1] Diesel engines are one of the main sources of air pollution in urban areas,[2] since they generate contaminants such as nitrogen oxides (NO_x) and particulate matter (PM).[3] Currently, environmental catalysis is especially focused on developing improved technologies to control the emissions of these pollutants, owing to the ever growing concern related to their harmful effects to both the environment and human health.[4] The implementation of a more stringent legislation for soot emissions has motivated the development of diverse strategies to control the emissions released by diesel engines.[5] These strategies can be classified into three groups: (i) modifications in the diesel engine designs, (ii) modifications of the fuel formulations and (iii) the use of filtering after-treatment devices.[6] Since it is foreseen that in order to accomplish the incoming legislation for regulating soot emissions neither the (i) nor (ii) strategies would be enough,[7] several after-treatment technologies have been proposed.[6]

Among the most effective after-treatment technologies developed to reduce the amount of soot released to the atmosphere, the use of DPFs (Diesel Particulate Filters) is found.[8] It is a wall-flow type monolith[6,9] which reduces particles emissions into the environment, minimizing the environmental hazards caused by diesel engines. The characteristic geometry of the DPF consists of half of the channels open at one extreme, whereas these open channels in one edge are closed at the opposite extreme. Therefore, the arrangement of the edge cross section looks like a checkerboard.[10] These filters provide channels into which the gas flows, but blocked ends force the incoming gases to pass through porous channel walls before they can exit the filter.[11] The constant filtration of the exhaust gases generates a progressive accumulation of soot, being required the filter regeneration by combustion of the retained soot.[5,12] The ignition of diesel particulate matter usually happens at 600 °C and the temperature of diesel exhaust gases ranges from 250 °C to 450 °C under normal working conditions, which is too low to begin the soot combustion spontaneously.[5,8,12] An extended regeneration strategy is the commercial CRT (Continuously Regeneration Trap) system.[13,14] This one consists of a DPF located downstream a Pt-containing DOC (Diesel Oxidation Catalyst). In the DOC the NO is oxidized to NO_2 and a continuous DPF regeneration takes place by the action of the NO_2, as NO_2 is more oxidant than O_2.[15] An

MCMA Group, Department of Inorganic Chemistry, Faculty of Sciences, University of Alicante, Ap.99 E-03080, Alicante, Spain. E-mail: a.garcia@ua.es; Fax: +34 96590 3454; Tel: +34 96590 9419

alternative and promising way to carry out the filter regeneration is using particulate filters containing a suitable catalyst to promote soot combustion.[6,13,16] Currently, one of the great challenges of the environmental catalysis is the development of a noble metal-free catalyst able to reduce the onset temperature of soot combustion, being ceria-based materials among the most promising active phases.[17] The key to understand the operation of these materials is based on their ability to release and store oxygen due to the redox couple Ce^{3+}/Ce^{4+}. Furthermore, the oxygen mobility in its lattice can be enhanced by inclusion of other cations, like zirconium or praseodymium, forming substitutional solid solutions, which can lead to non-stoichiometric mixed oxides. One of the most commonly used mixed oxides is ceria-zirconia ($Ce_xZr_{1-x}O_{2-\delta}$). The importance of these mixed oxides as catalysts has raised several studies for application to different oxidation reactions.[18–25] An enhancement of the catalytic properties of the cerium-based catalysts is achieved with the incorporation or dispersion of copper. Actually, cerium-based catalysts doped with copper have shown an exceptional activity, comparable to those exhibited by precious metals, towards some relevant reactions from a technological point of view; such as CO oxidation at low temperature, CO preferential oxidation in H_2-rich streams (CO-PROX) or the methanol synthesis from CO and H_2.[21,26–31] Recent studies point out an enhancement in terms of activity and selectivity in reactions such as NO oxidation to NO_2 and soot combustion when copper-doped cerium-based catalysts are used.[25,32]

The overall aim of this research is double: on the one hand, the feasibility in the incorporation of the active phase (2% CuO/$Ce_{0.8}Zr_{0.2}O_2$) to a commercial lab-scale diesel particulate filter (SiC-DPF) will be analyzed by using an alternative impregnation technique. It consists of achieving a well-adherent deposit of the catalyst directly on the ceramic structure (thus avoiding the adoption of intermediary washcoat) by using an environmentally-friendly impregnation technique, as it prescinds from surfactants or pH regulator agents. On the other hand, the catalytic activity of the catalyst supported onto the DPF towards NO oxidation and soot combustion reaction will be evaluated, being both key reactions in the framework of diesel decontamination. The reason for the addition of copper to the ceria-zirconia support, the choice of the particular formulation 2% CuO/$Ce_{0.8}Zr_{0.2}O_2$ and its influence both on the soot combustion activities and on the mechanism were properly described elsewhere.[25,33,34]

2. Experimental

Powder catalyst synthesis, characterization and testing

The 2% CuO/$Ce_{0.8}Zr_{0.2}O_2$ powder catalyst has been synthesized following a procedure based on the synthesis of $Ce_{0.8}Zr_{0.2}O_2$ mixed oxide and subsequent addition of the proper amount of copper by incipient wetness impregnation. A detailed description of the experimental procedure followed is described in the literature by Giménez-Mañogil *et al.*[25] The actual copper content on the catalyst was close to the nominal value, as verified by XRF technique.

$Ce_{0.8}Zr_{0.2}O_2$ and $Ce_{0.8}Zr_{0.2}O_2$-supported copper catalysts were then characterized. The specific surface areas of the samples were determined by the BET method. N_2 adsorption–desorption isotherms were obtained at −196 °C in an automatic volumetric system (Autosorb-6B from Quantachrome) after degassing the samples at 250 °C for 4 h. The specific pore volume was calculated from the desorption branch of the isotherm at $P/P_0 = 0.98$ following the criteria used by Moretti *et al.*[35]

Powder XRD patterns were recorded in a Bruker D8 advance diffractometer, using the CuKα radiation (λ = 0.15418 nm). Diffractograms were recorded between 10° and 60° (2θ) with a step size of 0.05° and measuring for 3 s at each step. Indexation and calculation of the unit cell parameter was performed by using the position of line (111) and Bragg's law, considering cubic system for ceria fluorite structure. The average crystal size estimation was carried out using Scherrer's equation. In order to improve accuracy, crystal sizes were estimated as an average value from those obtained from three representative fluorite reflections ((111), (220) and (311)).

Raman spectra were performed in a Bruker RFS 100/S Fourier Transform Raman Spectrometer with a variable power Nd:YAG laser source (1064 nm), 64 scans at 85 mW laser power (70 mW on the sample) were recorded and no heating of the sample was observed under these conditions.

The catalytic tests were performed in a tubular quartz reactor vertically positioned and coupled to specific NDIR-UV gas analyzers (Fisher-Rosemount, models BINOS 100, 1004, 1001) for CO, CO_2, NO, NO_2 and O_2 monitoring. For the NO oxidation tests, 80 mg of catalyst were diluted with 320 mg of SiC to avoid pressure drop. The gas mixture used comprised 500 ppm NO_x, 5% O_2 and balance N_2; the gas flow was fixed at 500 mL min^{-1} (GHSV = 30 000 h^{-1}). The experimental set-up has been designed in order to ensure that the proportion of NO_2 in the NO + O_2 mixture fed to the reactor is negligible, thus being similar to the proportion in the diesel exhaust. Catalytic tests consisted of Temperature Programmed Reactions (TPRs), where the temperature was increased from room temperature up to 700 °C at 10 °C min^{-1} under the reactive atmosphere, with the purpose of quantifying the NO to NO_2 oxidation capacity of the catalyst.

The NO_2 production profiles were determined in relation to the total amount of NO_x as a function of temperature.

The catalytic activity towards soot combustion was analyzed by means of Temperature Programmed Reactions (TPRs), which were carried out under identical experimental conditions than those used for the NO oxidation tests (but with soot). Additionally, the same gas mixture used for NO oxidation measurements was used for soot combustion tests. Soot conversion profiles were determined from the CO and CO_2 evolved. 80 mg of catalyst were mixed with the proper amount of Printex-U soot (supplied by Evonik-Degussa). As different soot–catalyst ratios were tested (1 : 6, 1 : 5, 1 : 4 and 1 : 3), both components were mixed in order to get both loose contact conditions (very gentle mixture of soot and catalyst with a spatula for 2–3 minutes) and tight contact conditions (intimate mixture of soot and catalyst in an agate mortar for 5–6 minutes), and they were diluted with the required amount of SiC to reach a final mass of 400 mg in the mixture.

Supported catalyst preparation, characterization and testing

The 2% CuO/$Ce_{0.8}Zr_{0.2}O_2$ was supported on lab-scale DPFs. The SiC wall-flow filters, which were used for this purpose, present the following geometrical characteristics: 7.5 cm in length, 2.5 cm of diameter, 300 cpsi, and an average porosity of 42%; they were provided by Céramiques Techniques et Industrielles. Before using them, the as-received DPFs were washed with water and acetone, dried at 110 °C and calcined at 700 °C for 2 h.

The catalyst incorporation on the surface of the filter channel inner walls was done using an easy and organic solvent-free procedure.

The ceramic support was vertically dipped in a dilute aqueous suspension of the as-prepared powder catalyst. The filter–suspension system was placed in an ultrasonic bath during 90 min. It must be noted that, taking into consideration the particular geometry of the substrate, the ceramic supports were turned upside down after waving the samples for the first 45 min. After the immersion, the samples were dried at 110 °C for 12 h and calcined at 600 °C for 2 h. The amount of catalyst loaded onto the DPF was determined by gravimetric difference.

One of the main advantages of this technique is that it is much greener than some others described in the literature, since water is used as solvent and it is devoid of surfactants and pH-regulators agents, which are chemicals that imply environmental concerns.[36–42]

In order to study the morphology of the catalyst anchored to the DPF walls, Scanning Electron Microscopy (SEM) was performed in a HITACHI S-3000N microscope with a secondary electron detector, a retrodispersed electron detector and X-ray detector (XFlash 3001 from Bruker) for microanalysis and chemical mapping. Previous to SEM characterization, a bare and a coated filter were cut into different pieces to examine the inner channel walls and cross sections.

The adherence of 2% CuO/$Ce_{0.8}Zr_{0.2}O_2$ coating on ceramic filters was evaluated by stressing the samples in an ultrasonic bath at ambient temperature. The coated filters were immersed in acetone inside a glass vessel, which was placed in an ultrasonic bath (Ultrasons P-selecta, 50–60 Hz) for 1 h.[40] After this treatment, the samples were dried overnight at 110 °C. In all cases, the coating adherence was determined by loss weight measurement.

The catalytic tests were performed using the same gas analyzers described for the powder catalysts. In this case, the employed reactor was a tubular stain steel reactor, 3 cm of inner diameter, and it was horizontally placed inside the furnace. The catalytic tests consisted of temperature programmed reactions, where the temperature was increased from room temperature up to 700 °C at 10 °C min^{-1} under the reactive atmosphere, with the purpose of quantifying the NO to NO_2 oxidation capacity of the catalyst. In order to study the thermal and chemical stability of the catalytic coating, after the first TPR run, the structured catalyst was cooled down in air and its catalytic capacity was evaluated again following the same procedure, which was repeated four consecutive times for the same coated DPF.

The catalyst's activity towards soot combustion once supported onto the DPF was analyzed by means of temperature programmed reactions, which were carried out under identical experimental conditions than those used for the NO oxidation tests (but with soot).

Previously, the filters were impregnated with soot by immersion into a soot–methanol suspension (7000 ppm) under vigorous stirring.[39] It must be noted that previous to the soot incorporation, the substrates were wrapped with Teflon to avoid the soot deposition onto the outside walls.[41] Finally, samples were dried at room temperature for 12 h. The soot loaded was gravimetrically determined. The average soot loaded over a coated filter was 0.075 ± 0.015 g, whereas an average of 0.090 ± 0.020 g of soot was incorporated over a bare filter.

3. Results and discussion

Powder catalyst characterization

Surface area values (S_{BET}) are shown in Table 1. The area of the copper containing catalyst is lower than that of the parent $Ce_{0.8}Zr_{0.2}O_2$ support. This lower value is in accordance with previous works related to samples prepared with the same procedure.[25,43]

The specific pore volume (V_s), calculated from the isotherms as described for this kind of materials, diminishes when copper is added.[35] These results indicate a certain ceria-zirconia's pores blocking upon copper incorporation on its surface.

Fig. 1 displays the X-ray diffractograms of the catalysts. Diffraction peaks attributable to cubic fluorite phase of ceria are observed in both samples. The diffraction peaks, characteristic of CuO phase (tenorite), were not detected, indicating that bulk CuO crystallites are not formed on this catalyst.

The symmetrical peaks of $Ce_{0.8}Zr_{0.2}O_2$ suggested formation of single ceria-zirconia solid solution (peak splitting would be expected if two phases were segregated). Table 1 lists lattice constants and average crystal sizes. As collected in Table 1, the lattice parameter estimated for the copper-containing catalyst is close to that of the support. This suggests that copper remains essentially on the surface, and it is not significantly

Table 1 Main parameters obtained from the textural and structural characterization

Catalyst	S_{BET} (m^2 g^{-1})	Lattice parameter (nm)	Average crystal size (nm)	Phases detected by XRD	F_{2g} band position (cm^{-1})	FWHM[a] (cm^{-1})
$Ce_{0.8}Zr_{0.2}O_2$	67	0.5362	5.5	Fluorite	473.5	60
2% CuO/$Ce_{0.8}Zr_{0.2}O_2$	49	0.5357	6.4	Fluorite	473.5	62

[a] Full width at half maximum for the F_{2g} Raman peak.

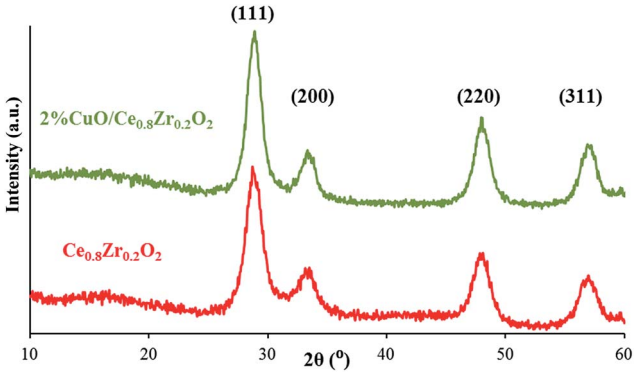

Fig. 1 XRD patterns for the catalysts (fluorite phase reflections are shown in parentheses).

incorporated into the fluorite structure, as could be promoted by other synthesis routes (*e.g.* micro emulsion-precipitation).[30,35,43]

The XRD patterns also showed very broad main peaks, suggesting, *a priori*, small crystal sizes. The determination of the crystal sizes can be approached by means of Scherrer's equation in agreement with Zhang *et al.*[44]

The mentioned average crystal sizes are also listed in Table 1, revealing that the value obtained for the copper-containing catalyst (6.4 nm) remains close to that of the parent ceria-zirconia support (5.5 nm).

The XRD results are well complemented by the Raman study. Fig. 2 shows the Raman spectra of the samples, all with a main band at 473.5 cm^{-1} ascribed to the F_{2g} vibration mode of the fluorite structure of ceria. The intensity of this band decreases with the loading of copper, which could be related to the optical absorption of copper, as discussed elsewhere.[25] However, it must be taken into account that the presence of copper neither affects the F_{2g} band position at 473.5 cm^{-1} nor the band broadening (Table 1). Results reveal that copper is not inserted into the ceria-zirconia lattice or there is a small incorporation of copper at surface or subsurface positions of the lattice; which might not be detected by Raman spectroscopy for this catalyst. Copper incorporation into the lattice would have been detected by red shift and broadening of the main F_{2g} mode, as published by Gamarra *et al.*[43]

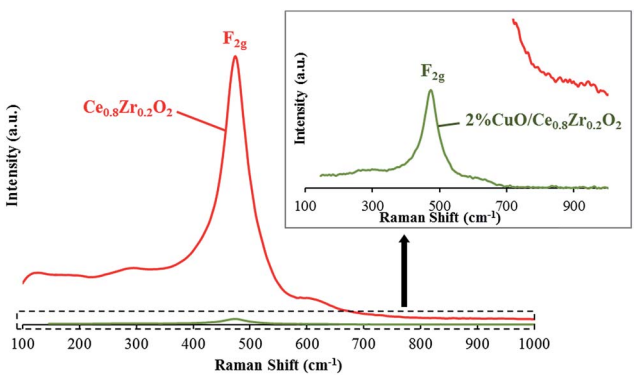

Fig. 2 Raman spectra of the catalysts (inset: zoom for 2% CuO/$Ce_{0.8}Zr_{0.2}O_2$ sample spectrum).

Finally, very low intensity Raman bands have been found at ≈120 cm^{-1} and 292 cm^{-1} for the ceria-zirconia support, which can be associated to Zr incorporation into the ceria lattice with the consequent distortion of the framework symmetry. Additionally, the weak and broad band extending between 560 and 650 cm^{-1} can be associated to the presence of oxygen vacancies.[43,45,46]

Incorporation of the active phase to the DPF substrate

As described previously, the main goal of this research is to study the catalytic performance of 2% CuO/$Ce_{0.8}Zr_{0.2}O_2$ once supported on a diesel particulate filter. Therefore, a preceding step consisting of incorporating the active phase onto a DPF substrate is required. The impregnation procedure carried out must ensure a simple, controlled and reproducible incorporation of the as-prepared catalyst. Another parameter to take into consideration is the amount of catalyst incorporated, since it should be optimum, thus yielding a satisfactory catalytic activity without blocking the porosity of the channel walls.

The designed procedure to carry out the incorporation of the active phase onto the DPF is based on using an aqueous solution as impregnation agent. This impregnation procedure was accomplished over nine DPFs.

The obtained results point out a satisfactory impregnation reproducibility, as the gained weight average value over those 9 DPFs is 0.4425 g (approximately 1.4% DPF weight), with a standard deviation of 7.2%. It must be noted that this amount of catalyst does not block the channel wall pores, as proved by forcing a gas flow of 500 mL min^{-1} to go through the loaded DPF and checking that this gas flow did not diminish at the DPF exit. It can be concluded that pressure drop will not be relevant during the catalytic tests.

Supported catalyst characterization

The scanning electron microscopy technique allows us the study of the active phase's morphology. In order to analyze the distribution of the active phase on the channel walls, SEM images of an active phase-coated DPF were compared with those obtained from a bare DPF. Previous to SEM characterization, both coated and uncoated DPFs were cut into different pieces for two reasons: the whole DPF exceeds the sample size that can be analyzed by the available equipment and to obtain images from the channel inner walls of the DPF.

Fig. 3 schematizes the different DPF pieces obtained in order to be analyzed by SEM. As seen in Fig. 3b and c, two consecutive cross sections (1 cm thickness) were cut, corresponding to the DPF edge and the immediately adjacent cross section. The longitudinal section of the remaining DPF piece was analyzed as well, as schematized in Fig. 3d.

Fig. 4 shows micrographs of the bare substrate (from the longitudinal section, see Fig. 3d). The wall surface can be seen in detail in Fig. 4a, and the wall cross section in Fig. 4c. Both images exhibit a globular morphology, leading to a high porosity between SiC grains. The comparison between Fig. 4a and c allows us to observe a higher porosity in the wall cross section regarding the wall surface. As seen in Fig. 4c the pores

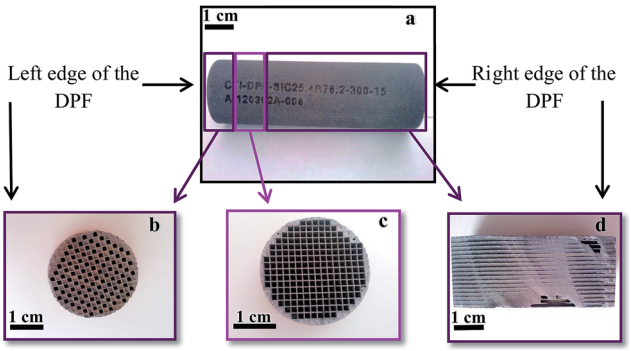

Fig. 3 Pictures (a) whole filter, previous to its fragmentation. (b) External cross section of the filter. (c) Inner cross section of the filter. (d) Longitudinal cross section of the remaining filter.

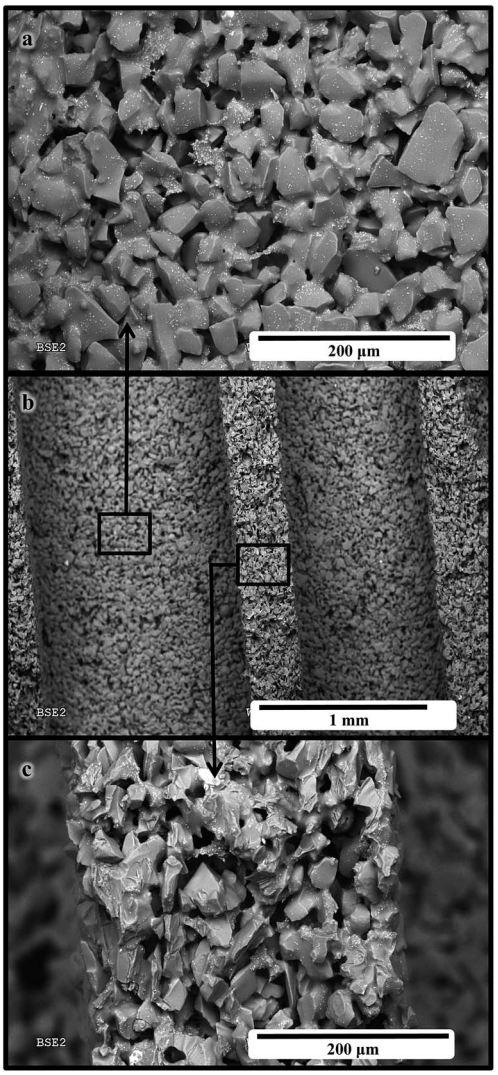

Fig. 4 Micrographs of the structured substrate: (a) 250×, (b) 45× and (c) 250×.

are well-connected among them, being observed the characteristic flow-pass structure inside the wall, which is required to achieve a high filtration efficiency of the diesel exhaust.

Fig. 5 shows micrographs obtained from the most external cross section (see Fig. 3b) of a coated DPF. As observed, the active phase was incorporated to the DPF through the DPF open channel. A more abundant agglomeration of active phase is observed at the corners of the channel, as previously observed by other authors.[41] Fig. 5c shows in more detail an accumulation of active phase deposited on the channel walls.

Fig. 6 shows SEM images obtained from the inner cross section of a loaded DPF corresponding to the cut showed in Fig. 3c. As observed in Fig. 6b, all the channels are open, as it is the inner cross section. It was assumed that the impregnation process of the substrate was governed by action of both capillarity and gravity.[37,39] Moreover, as the designed impregnation process is based on the filters' immersion in an aqueous solution, followed by a 180° rotation of the DPF position regarding its longitudinal axis and subsequent immersion, it is expectable the presence of active phase anchored onto all the DPF's channels. In this sense, it is reasonable to find a lower active

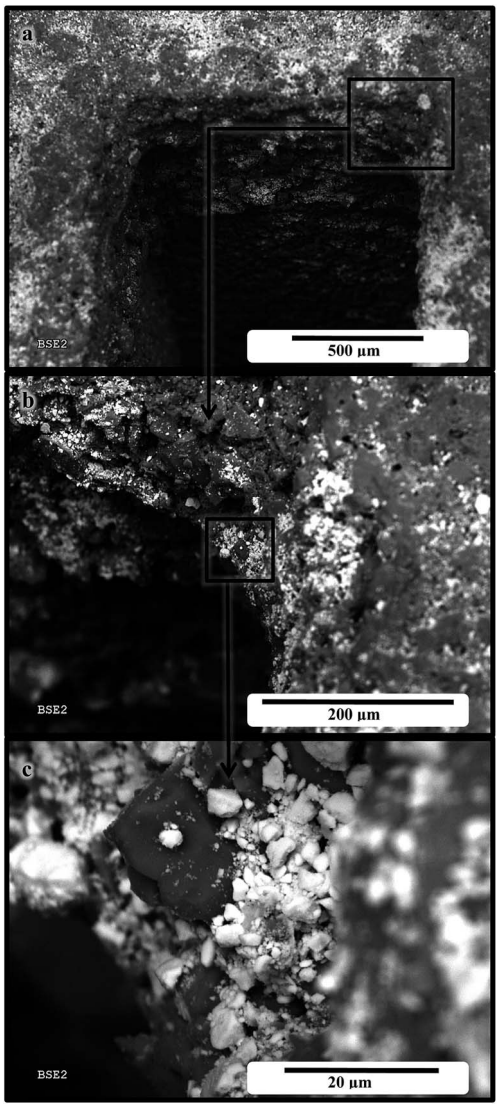

Fig. 5 Micrographs of the external cross section of a loaded DPF: (a) 70×, (b) 250× and (c) 2000×.

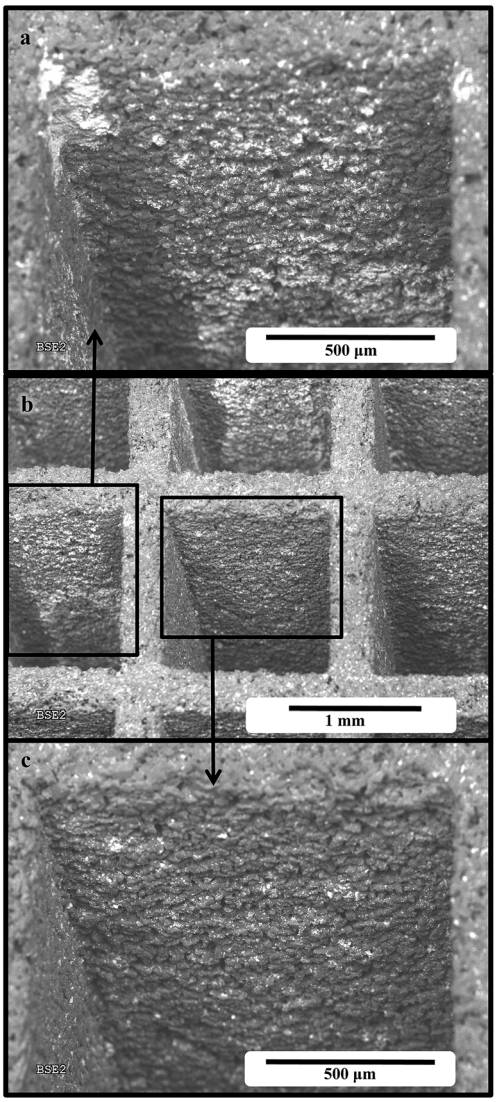

Fig. 6 Micrographs of the inner cross section of a loaded DPF: (a) 35×, (b) 90× and (c) 90×.

phase concentration near the DPF's closed edges, as in these regions the catalyst solution will only arrive by gravity effect. To state that hypothesis, it was assumed that the aqueous suspension ascent through the channels by capillarity action is more disfavored than the suspension descent by gravity effect.

The rotation step during the impregnation process was performed to ensure an equivalent catalyst loading over the open channels, independently on the DPF extreme, and the same in the case of the closed channels. Taking into account the former hypothesis, it is expected to obtain a higher concentration of active phase in those regions closer to the open channels' edge. As seen in Fig. 6b, there is active phase anchored in every channel. As expected, a higher concentration of active phase is observed in alternate channels, which correspond to the open channels. On these channels the catalyst-containing solution is arriving through two different mechanisms, capillarity and gravity. However, for the channels whose edges are closed, the active phase will only arrive by gravity action, since the path to be followed by the solution is much longer than that followed by capillarity action. In conclusion, the active phase distribution, for the same channel, differs significantly between the open and the closed edge, being higher the active phase concentration onto the open edge than that on the closed one.

Fig. 7a and 8a show the same micrograph of the channel inner walls of two consecutive channels (observed from the longitudinal section, see Fig. 3d). Fig. 7 is focused on the left channel (Fig. 7a), which shows a higher concentration of active phase since this channel is near the open edge of the filter. Fig. 8 is focused on the right channel (Fig. 8a), which shows a lower concentration of active phase since this channel is near the closed edge of the filter. It was verified a higher catalyst loading at the open channels regarding the closed ones, as a consequence of the particular geometry and design of the substrate. As seen, the catalyst is well-spread along the channel walls, nevertheless it is not forming a continuous layer, since the incorporated catalyst mass is too low to cover all the DPF channels' surface.

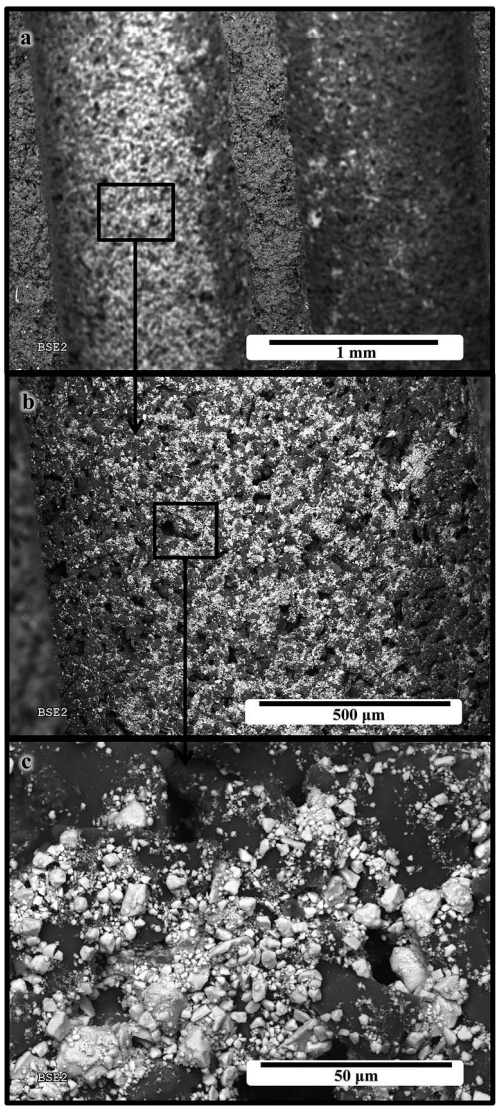

Fig. 7 Morphology of the coated catalyst. View of the channel surface: (a) 45×, (b) 100× and (c) 1000×.

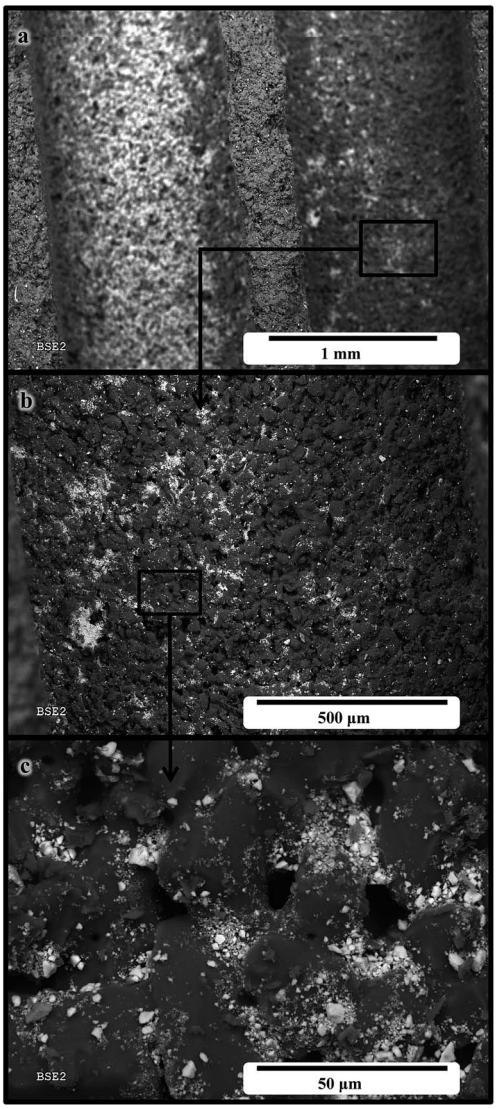

Fig. 8 Morphology of the coated catalyst. View of the channel surface: (a) 45×, (b) 100× and (c) 1000×.

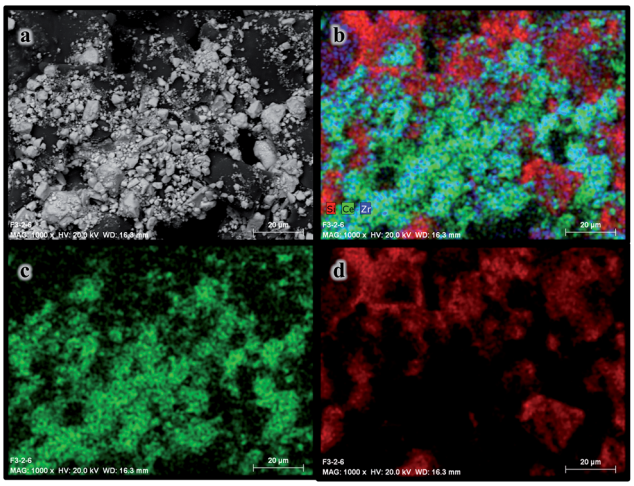

Fig. 9 SEM-chemical mapping analysis of the left channel showed in Fig. 7a and 8a: (a) SEM picture, (b) Si (red)–Ce (green)–Zr (blue) analysis, (c) Ce analysis (green) and (d) Si analysis (red).

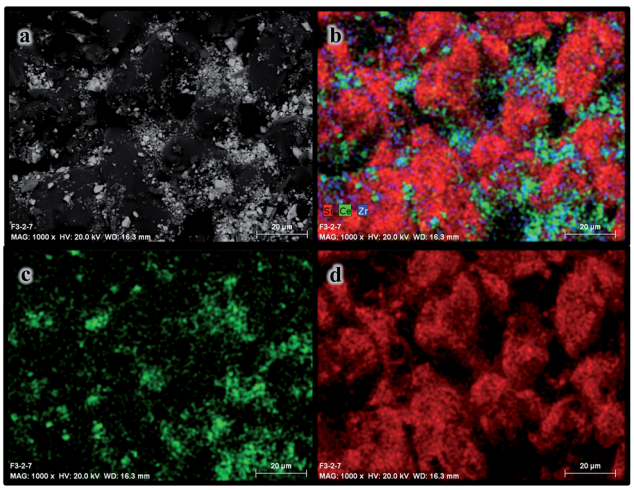

Fig. 10 SEM-chemical mapping analysis of the right channel showed in Fig. 7a and 8a: (a) SEM picture, (b) Si (red)–Ce (green)–Zr (blue) analysis, (c) Ce analysis (green) and (d) Si analysis (red).

SEM-chemical mapping shown in Fig. 9 and 10 was performed over the channel with the highest loading of active phase and the consecutive channel with a lower content of active phase, respectively. It is useful to analyze the distribution of the different components of the coating after being anchored onto the substrate. Fig. 9a exhibits a SEM micrograph of the channel on the right side (shown in Fig. 7a). Additionally, the Ce distribution, which has been selected as representative element of the active phase, and the Si distribution, selected as representative element of the silicon carbide substrate, are also included in Fig. 9c and d, respectively. The distribution of Si (red), Ce (green) and Zr (blue) were also included in Fig. 9b. For comparative purposes, Fig. 10 shows the same representative images for the channel on the left shown in Fig. 7a.

It is observable that there is active phase onto both channels, hence it can be concluded that the active phase was incorporated onto all the channels. However, if Fig. 9 and 10 are compared, a poorer distribution of cerium and zirconium over the channel with a lower loading of active phase is observed.

Mechanical stability

These coated substrates are proposed to be used in the vehicles' exhaust pipes; consequently, it is essential to have a good mechanical stability. In order to analyze the mechanical stability of the catalytic coating, the weight loss was measured after stressing the samples 60 min in an ultrasonic bath (which allows simulating engine vibrations under operation). This coating adherence test was performed over three different coated DPFs. After drying the samples, a weight loss lower than 4% of the 2% $CuO/Ce_{0.8}Zr_{0.2}O_2$ amount was observed for all the cases.

The satisfactory coating adherence can be related to the high external porosity and roughness of the substrate walls (with an

average porosity value of 42.6%), which provides many sites for the catalytic coating anchoring.[37]

Catalytic oxidation of NO to NO_2

Fig. 11 shows the NO_2 production profiles obtained in the catalytic tests performed without soot. In order to analyze the catalytic behavior of 2% CuO/ceria-zirconia/DPF catalyst in the NO oxidation reaction, the activity of this sample was compared with a bare DPF (non-catalyzed reaction) and 2% CuO/ceria-zirconia powder catalyst.

As observed in Fig. 11, in presence of catalyst, the NO oxidation to NO_2 is improved with regard to the non-catalyzed reaction, decreasing the onset reaction temperature and shifting the maximum oxidation temperature towards lower values. Concerning the catalyzed/SiC-DPF reaction, a maximum value around 40% NO_2 was found at 400 °C, while this value was 6% at 470 °C for the bare DPF. The results show a very high activity of the active phase-loaded DPF towards the NO oxidation reaction, pointing out a satisfactory catalytic performance of the catalytic-coated filter, despite the non-continuous dispersion of the catalyst along the channel walls.

The evaluation of the catalytic coating stability was performed by successive NO oxidation cycles. Therefore, the catalytic coating capacity for being reused and the possible deactivation of catalytic system were studied. As seen in Fig. 11, there are small differences from the first to the fourth NO_2 production cycle, with a slight increment in the NO_2 production for the second cycle regarding the first one, trend not followed by the third and fourth cycles, which are very similar. The general pattern of these NO oxidation profiles is composed of: (i) a minor contribution of NO_2 desorption at low temperatures (in the range of 100–200 °C) due to oxidation/desorption of previous ad-NO_x species on solid's surface at low temperatures and (ii) the NO_2 production profile controlled by the thermodynamic equilibrium of NO oxidation (gas phase) at high temperatures.

A minor detail which should be commented is the irregular profile appearing at 300 °C in the first cycle (as a "kink") and becoming much more attenuated for the subsequent cycles. A tentative explanation for that could be an accentuated and punctual production of NO_2 by an abrupt decomposition of nitrites/nitrates[47] and/or decarbonation of the ceria-based solid[48] followed by fast production and decomposition of NO_2-forming species. It is important to remember that the amount of catalyst is higher for the experiment with the coated DPF than that with the powder catalyst (400 mg *versus* 80 mg) and that it is dealing with the fresh catalyst in the first cycle. This last idea could tentatively account for the slight increase in NO_2 production from the first to the second cycle. Minimum drop from the second to the third area could be attributed to slight lowering in BET surface area because of the temperature cycles.

As a brief summary, the TPR results indicate that there is no catalytic deactivation during the different cycles. Hence, this catalytic system can be reused in several cycles without a significant loss in activity at least up to 700 °C.

On the other hand, the active phase must fulfill some requirements if this catalytic system, consisting of a coated DPF, is meant to be used as an after-treatment device in diesel engines. In this regard, the catalytic coating must show a high thermal and chemical stability. Some authors have evidenced that the temperature inside the DPF can increase up to 1000–1100 °C during the DPF regeneration, as a consequence of the highly exothermal soot combustion process;[49] consequently, a high thermal shock resistance should be achieved by this catalytic system. Some authors suggest temperature gradients of 100 °C cm^{-1} along both radial and longitudinal directions of the DPF.[49] Successive NO oxidation cycles allow us the evaluation of thermal and chemical stability and also thermal shock resistance; as the sample is being heated progressively, using a high heating rate (10 °C min^{-1}), in the presence of a highly oxidant atmosphere. Based on the similitude among the four successive NO_2 production cycles, it can be concluded that a

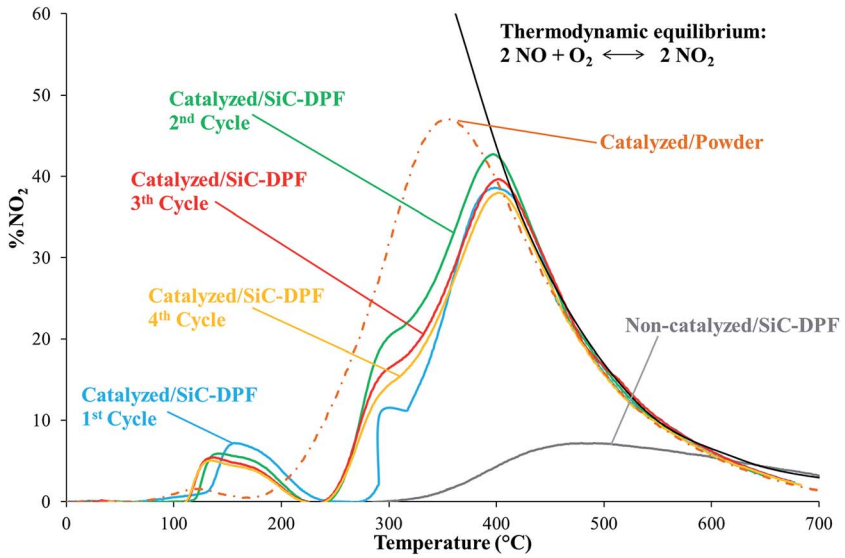

Fig. 11 NO_2 production profiles under TPR conditions. Solid lines: successive cycles with the same loaded DPF (1st–4th).

high thermal and chemical stability characterizes this catalytic system.

Even though the NO_2 production profile showed by the powder catalyst has been included in the same figure, a direct comparison among these profiles is not possible, due to the differences between gas space velocities (GHSV) when different catalyst configurations are employed, as the catalyst bed volume is not equal in both cases. However, the powder catalyst profile is included in Fig. 11 to establish a comparison between the profiles' shapes. The absence of significant differences between both profiles, independently on the catalyst configuration, points out a satisfactory catalytic activity towards NO oxidation reaction of the coated DPF, even when there are dramatic differences between both catalytic configurations.

It is worthwhile to evaluate the NO oxidation capacity of the catalytic coating, since this reaction plays a key role in the beginning and continuity of soot combustion reaction, as previously reported by some authors.[19,50]

Catalytic soot combustion

The aims of this section are: firstly, to verify the catalytic performance of the supported catalyst onto the DPF towards the soot combustion reaction; secondly, to study the contact extent established between soot and catalyst after their incorporation onto the DPF. In order to achieve the latter aim, two contact modes between the soot and the powder catalyst were employed, loose and tight. Afterwards, the soot combustion profile obtained with the supported catalyst will be compared with those obtained from both contact modes (powder catalyst–soot).

It should be noted that there are dramatic differences in the gas space velocities (GHSV) between both reactor catalyst configurations, since a real scale-up is not possible owing to the own limitations of the experimental set-up. Therefore, in an attempt to conduct a proper comparison between the soot combustion profiles, an identical soot–catalyst ratio must be established in all the experiments. Consequently, a preliminary study of the influence of the soot–catalyst ratio over the soot combustion rate was performed. Hence, soot combustion experiments under TPR conditions were carried out with the powder catalyst, using mixtures with different soot–catalyst ratios. All the experiments were performed using the same amount of catalyst (80 mg) under loose contact conditions.

Fig. 12 illustrates the soot combustion curves, being included the inset zoom at low/medium temperatures and low values of conversion. It is interesting to note that the soot–catalyst ratios of 1 : 6, 1 : 5 and 1 : 4 show very close T_{50} values among each other. However, the curve obtained with the 1 : 3 ratio is shifted to higher temperatures. Therefore, the soot–catalyst ratio selected to perform the experiment has an influence over the soot combustion curve. This influence is not observed for the whole range of soot–catalyst ratios; in fact, the results depicted in Fig. 12 show that only for the highest soot–catalyst ratio the soot combustion curve shifts towards higher temperatures, thus showing a lower catalytic activity. These results are in accordance with those previously published in the literature by Peralta *et al.*[51] They suggested that not all the soot particles are in complete contact with the catalyst particles, so at a certain point of soot conversion there is an important loss in the extent of the soot–catalyst contact, being more critical at high soot–catalyst ratios and therefore a lower reaction rate is observed.

Taking into consideration the previous results, soot–catalyst ratios higher than 1 : 4 should be avoided as they lead to lower catalytic activities. The chosen soot–catalyst ratio to carry out all the experiments is 1 : 5.

Fig. 13 shows the TPR experiments carried out with the catalyst in both configurations: powder and supported. The soot

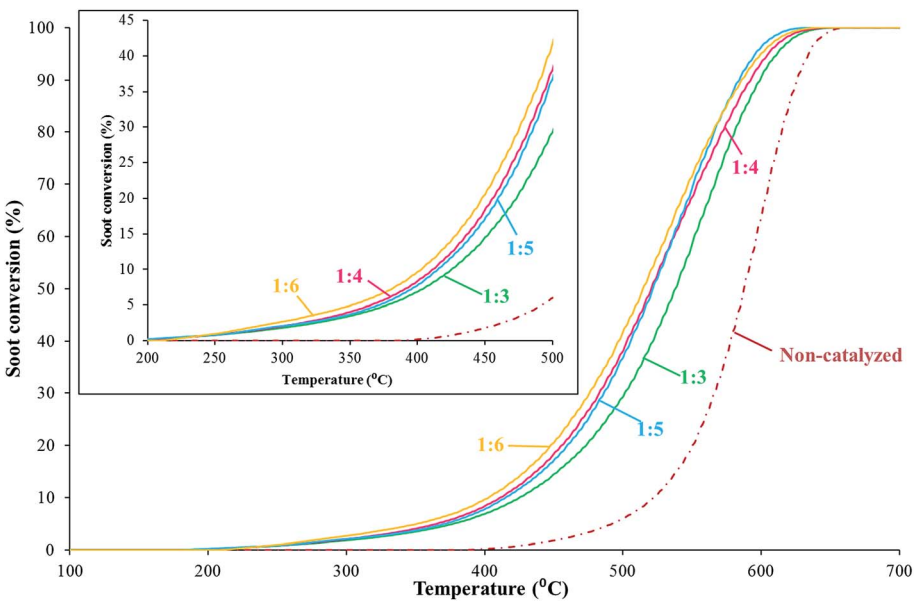

Fig. 12 Soot combustion curves *versus* temperature for different soot–catalyst ratios (inset: the detail at low and medium temperatures).

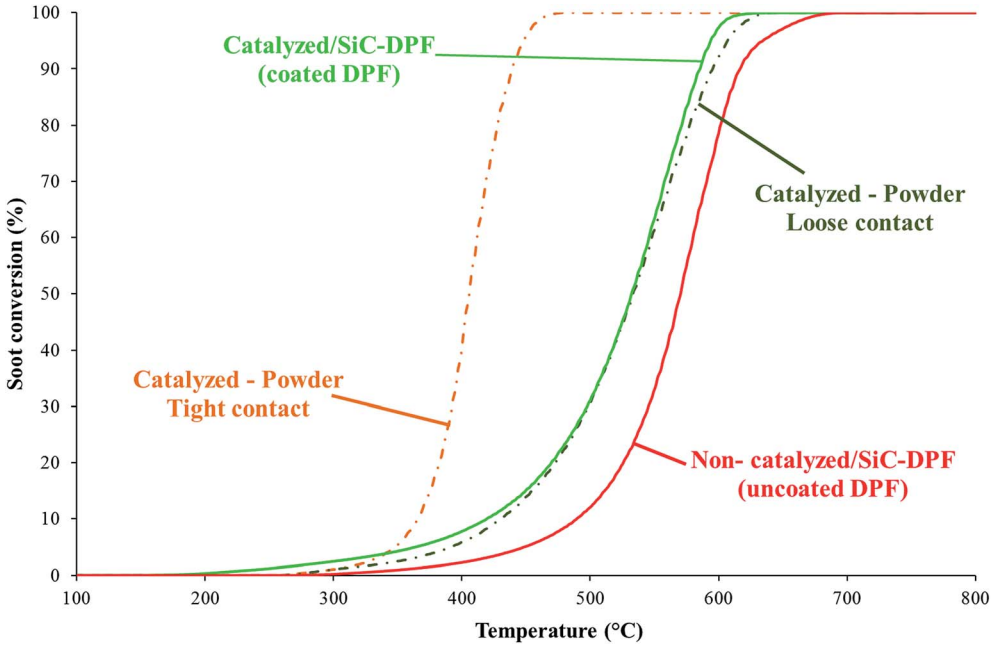

Fig. 13 Soot combustion curves *versus* temperature under TPR conditions for different catalytic configurations (soot–catalyst ratio 1 : 5).

conversion profile obtained for the bare DPF is plotted in the same figure.

The soot conversion curve shows a significant shift towards lower temperatures when the supported catalyst is used (regarding the non-catalyzed reaction with a bare DPF), as depicted in Fig. 13. These results revealed a high activity shown by the loaded DPF if compared with the unloaded DPF. The in-depth analysis of the soot combustion profiles points out that at low temperatures a better soot–catalyst contact degree is established in the DPF comparing the powder mixture, as the onset temperature is lower when the supported catalyst is used (161 °C) if compared with the powder catalyst (262 °C), and the same trend is observed at high temperatures. A possible hypothesis to explain this behavior is that the catalyst supported onto the DPF is well-spread along the DPF channel walls, leading to a more favorable contact between catalyst and soot than that established when the powder catalyst is employed. Based on these results, it is proved that for carrying out the elimination of soot at low temperature, the supported catalyst configuration is more favorable than the powder catalyst configuration.

On the other hand, the study of the catalytic results gained when the powder catalyst is employed, revealed that the temperature at which the profiles appear is strongly influenced by the contact degree between catalyst and soot. It can be seen that when soot and catalyst are very gently mixed (with a spatula), the soot combustion profile is shifted to higher temperatures than when soot and catalyst are mixed intimately (in an agate mortar), with a T_{50} value of 406 °C in tight contact mode and 532 °C when loose contact is employed; being the degree of contact between soot and catalyst critical in the context of this reaction.

In order to shed some light on the contributions of NO_2-assisted soot combustion and "active oxygen"-assisted soot combustion, Fig. 14 depicts the NO_2 slip percentage in terms of temperature for the configurations compiled in Fig. 13. This parameter reflects (at least if the NO ↔ NO_2 recycling efficiency is not very high) how NO_2 is specifically used for the soot combustion reaction. As can be observed, the soot–catalyst degree of contact strongly influences the NO_2 slip profiles. Due to the synergy between the above-mentioned mechanisms, and as a consequence of the combustion progress (soot surface is becoming more and more populated of oxygen surface groups), NO_2 is used more efficiently for the soot combustion under the tight contact mode (complete NO_2 removal at 400 °C, when combustion rate is high, and only NO_2 emerges when soot has been practically consumed). Conversely, the other two configurations exhibit "parallel" NO_2 slip profiles and whatever the reaction temperature, NO_2 always slips, thus revealing that under these both situations (coated DPF and loose-contact) NO_2

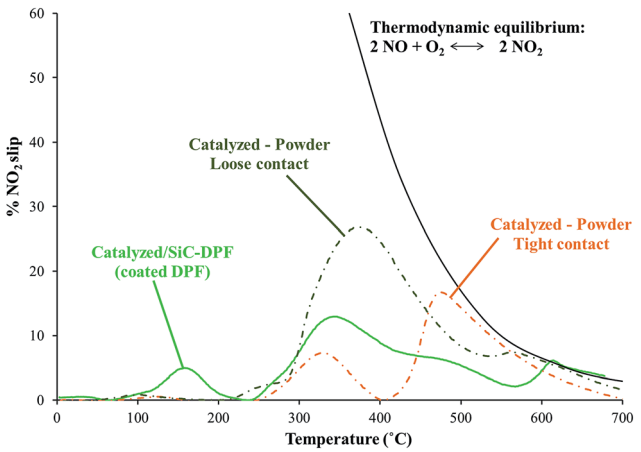

Fig. 14 NO_2 slip profiles in TPR soot combustion experiments.

production is not the rate-limiting step. These results are in agreement with those previously published by the authors[19,50,52] concerning the prevalence and synergies of both mechanisms in the soot combustion context.

It should be remarked that the soot combustion profile obtained with the powder catalyst under loose contact conditions is quite similar to that obtained with the loaded filter; being verified the good choice of conducting catalytic experiments under loose contact conditions when the powder catalyst is used, in order to simulate the performance of this type of catalysts in a diesel particulate filter. On the contrary, the soot conversion profile obtained under tight contact conditions is very far from those mentioned above, and consequently, does not simulate the real physical contact achieved in a diesel particulate filter. These results are in accordance with those previously published by Neyertz *et al.*[39]

4. Conclusion

This research was dedicated to the incorporation of the active phase onto a diesel particulate filter following a simple and green procedure, and the study of the catalytic activity of 2% CuO/ceria-zirconia catalyst supported onto a DPF. The general conclusions that were drawn are the following:

• The catalyst incorporation onto the diesel particulate filters was successfully achieved by using a simple and green procedure. Furthermore, the amount of catalyst incorporated is controllable and reproducible.

• An important feature of the synthesized catalyst is its high coating adherence, a needed requirement that must be fulfilled if these coated substrates are going to be integrated in exhaust pipes.

• The morphology adopted by the supported catalyst onto the DPF is a non-continuous deposit over the channel inner walls. Therefore, this non-homogeneous distribution avoids the channels porosity blocking. In addition, the catalytic coating showed a satisfactory activity towards NO oxidation reaction and soot combustion reaction.

• The catalytic coating exhibited an excellent thermal and chemical stability towards NO oxidation reaction. Consequently, the same coated DPF can be reused in several oxidation cycles without a significant loss in its catalytic activity.

• It was checked a satisfactory catalytic activity of the supported catalysts towards soot combustion. It was verified that loose-contact mode is a good choice to simulate the catalytic performance of this active phase in a diesel particulate filter, as well.

Acknowledgements

The authors gratefully acknowledge the financial support of Generalitat Valenciana (PROMETEOII/2014/010 project), the Spanish Ministry of Economy and Competitiveness (CTQ2012-30703 project, UE-FEDER funding). S.Q.D. wishes to thank VIDI-University of Alicante her Master Thesis Grant.

References

1 J. Fenger, *Atmos. Environ.*, 1999, **33**, 4877–4900.
2 J.-H. Tsai, S.-Y. Chang and H.-L. Chiang, *Atmos. Environ.*, 2012, **61**, 499–506.
3 J. P. A. Neeft, M. Makkee and J. A. Moulijn, *Fuel Process. Technol.*, 1996, **47**, 1–69.
4 A. Setiabudi. Ph.D. thesis, Technological University of Delft, 2004.
5 D. Fino, *Sci. Technol. Adv. Mater.*, 2007, **8**, 93–100.
6 D. Fino and V. Specchia, *Powder Technol.*, 2008, **180**, 64–73.
7 M. V. Twigg, *Catal. Today*, 2011, **163**, 33–41.
8 M. Jeguirim, V. Tschamber and J. F. Brilhac, *J. Chem. Technol. Biotechnol.*, 2009, **84**, 770–776.
9 J. M. Trichard, *Stud. Surf. Sci. Catal.*, 2007, **171**, 211–233.
10 M. A. Mokhri, N. R. Abdullah, S. A. Abdullah, S. Kasalong and R. Mamat, *Procedia Eng.*, 2012, **41**, 1750–1755.
11 A. P. Walker, *Top. Catal.*, 2004, **28**, 1–4.
12 B. A. A. L. van Setten, M. Makkee and J. A. Moulijn, *Catal. Rev.: Sci. Eng.*, 2001, **44**, 489–564.
13 M. V. Twigg, *Appl. Catal., B*, 2007, **70**, 2–15.
14 M. V. Twigg, *Catal. Today*, 2006, **117**, 407–418.
15 M. Valencia, E. López, S. Andrade, N. Guillén-Hurtado, V. Rico-Pérez, A. García-García, C. Salinas Martínez de Lecea and A. Bueno-López, *Top. Catal.*, 2013, **56**, 452–456.
16 P. Zelenka, W. Cartellieri and P. Herzog, *Appl. Catal., B*, 1996, **10**, 3–28.
17 A. Bueno-López, *Appl. Catal., B.*, 2014, **146**, 1–11.
18 A. Trovarelli, *Catalysis by Ceria and Related Materials, Catalytic Science Series*, Imperial College Press, vol. 2, 2002.
19 N. Guillén-Hurtado, A. Bueno-López and A. García-García, *Appl. Catal., A*, 2012, **437–438**, 166–172.
20 N. Guillén-Hurtado, A. Bueno-López and A. García-García, *J. Mater. Sci.*, 2012, **47**, 3204–3213.
21 E. Aneggi, C. de Leitenburg and A. Trovarelli, *Catal. Today*, 2012, **181**, 108–115.
22 L. Liu, Z. Yao, B. Liu and L. Dong, *J. Catal.*, 2010, **275**, 45–60.
23 A. E. Nelson and K. H. Schulz, *Appl. Surf. Sci.*, 2013, **210**, 206–221.
24 N. Guillén-Hurtado, I. Atribak, A. Bueno-López and A. García-García, *J. Mol. Catal. A: Chem.*, 2010, **323**, 52–58.
25 J. Giménez-Mañogil, A. Bueno-López and A. García-García, *Appl. Catal., B*, 2014, **152–153**, 99–107.
26 A. Jia, G. Hu, L. Meng, Y. Xie, J. Lu and M. Luo, *J. Catal.*, 2012, **289**, 199–209.
27 A. Martínez-Arias, M. Fernández-García, J. Soria and J. C. Conesa, *J. Catal.*, 1999, **182**, 367–377.
28 A. Martínez-Arias, D. Gamarra, M. Fernández-García, X. Q. Wang, J. C. Hanson and J. A. Rodríguez, *J. Catal.*, 2006, **240**, 1–71.
29 A. Martínez-Arias, A. B. Hungría, M. Fernández-García, J. C. Conesa and G. Munera, *J. Phys. Chem. B*, 2004, **108**, 17983–17991.
30 A. Martínez-Arias, D. Gamarra, M. Fernández-García, A. Hornés, P. Bera, Z. Koppány and Z. Schay, *Catal. Today*, 2009, **143**, 211–217.

31 Z. Y. Pu, X. S. Liu, A. P. Jia, Y. L. Xie and J. Q. Lu, *J. Phys. Chem. C*, 2008, **112**, 15045–15051.
32 F. Lin, X. Wu and D. Weng, *Catal. Today*, 2011, **175**, 124–132.
33 N. Guillén-Hurtado. Ph.D. thesis, University of Alicante, 2013.
34 J. Giménez-Mañogil and A. García-García, *Fuel Process. Technol.*, 2015, **129**, 227–235.
35 E. Moretti, L. Storaro, A. Talon, M. Lenarda, P. Riello, R. Frattini, M. Martinez de Yuso, A. Jiménez-López, E. Rodríguez-Castellón, F. Ternero, A. Caballero and J. P. Holgado, *Appl. Catal., B*, 2011, **102**, 627–637.
36 D. Mescia, J. C. Caroca, N. Russo, N. Labhsetwar, D. Fino, G. Saracco and V. Specchia, *Catal. Today*, 2008, **137**, 300–305.
37 S. Biamino, P. Fino, D. Fino, N. Russo and C. Badini, *Appl. Catal., B*, 2005, **61**, 297–305.
38 V. Rico-Pérez, S. Parres-Esclapez, M. J. Illán-Gómez, C. Salinas-Martínez de Lecea and A. Bueno-López, *Appl. Catal., B*, 2011, **107**, 18–25.
39 C. A. Neyertz, E. E. Miró and C. A. Querini, *Chem. Eng. J.*, 2012, **181–182**, 93–102.
40 C. A. Neyertz, E. D. Banús, E. E. Miró and C. A. Querini, *Chem. Eng. J.*, 2014, **248**, 394–405.
41 E. D. Banús, V. G. Milt, E. E. Miró and M. A. Ulla, *Appl. Catal., B*, 2013, **132–133**, 479–486.
42 L. E. Gómez, I. S. Tiscornia, A. V. Boix and E. E. Miró, *Int. J. Hydrogen Energy*, 2012, **37**, 14812–14819.
43 D. Gamarra, G. Munuera, A. B. Hungría, M. Fernández-García, J. C. Conesa, P. A. Midgley, X. Q. Wang, J. C. Hanson, J. A. Rodríguez and A. Martínez-Arias, *J. Phys. Chem. C*, 2007, **111**, 11026–11038.
44 F. Zhang, Q. Jin and S. Chan, *J. Appl. Phys.*, 2004, **95**, 4319–4326.
45 J. L. Ayastuy, A. Gurbani, M. P. Gónzalez-Marcos and M. A. Gutiérrez-Ortiz, *Int. J. Hydrogen Energy*, 2012, **37**, 1993–2006.
46 J. L. Ayastuy, A. Gurbani, M. P. Gónzalez-Marcos and M. A. Gutiérrez-Ortiz, *Int. J. Hydrogen Energy*, 2010, **35**, 1232–1244.
47 I. Atribak, A. Bueno-López and A. García-García, *Appl. Catal., B*, 2009, **92**, 126–137.
48 I. Atribak, A. Bueno-López, A. García-García and B. Azambre, *Phys. Chem. Chem. Phys.*, 2010, **12**, 13770–13779.
49 N. Miyakawa, H. Sato, H. Maeno and H. Takahashi, *JSAE Rev.*, 2003, **24**, 269–276.
50 I. Atribak, F. E. López-Suárez, A. Bueno-López and A. García-García, *Catal. Today*, 2011, **176**, 404–408.
51 M. A. Peralta, M. S. Gross, B. S. Sánchez and C. A. Querini, *Chem. Eng. J.*, 2009, **152**, 234–241.
52 N. Guillén-Hurtado, F. E. López-Suárez, A. Bueno-López and A. García-García, *React. Kinet., Mech. Catal.*, 2014, **111**, 167–182.